First Principles and Experimental Study on Photocatalytic Adsorption Property of SnO_2@CuO Core-shell Structure

Kangying LI [1], Jiale HUANG [1, 2], Xiao ZHANG [1, 3], Xiaolong ZHOU [1] *

[1] *Faculty of Materials Science and Engineering / Key Laboratory of Advanced Materials of Yunnan Province, Kunming University of Science and Technology, Kunming, 650093, China*
[2] *Jiangxi Acichemshun Industry Co. Ltd, Jiangxi, 337000, China*
[3] *Antai Tianlong Tungsten & Molybdenum Technology Co., Tianjin, 10094, China*

http://doi.org/10.5755/j02.ms.40258

Received 31 January 2025; accepted 11 April 2025

The structural stability, electronic properties and catalytic performance of SnO_2 nanoclusters, CuO nanoclusters and SnO_2@CuO core-shell structure were investigated by density functional theory. Compared with the single SnO_2 and CuO, the electronic states of both the core and the shell layer of the core-shell structure are reduced, which is favorable to the stability of the core-shell structure and the ionic bond formation between the core and the shell layer is favored; as shown by the charge transfer state, the CuO shell layer potential is reduced and the surface activity is increased, while the SnO2 core potential is increased and the surface activity is reduced, the shell layer can better encapsulate the core, and the SnO_2@CuO core-shell structure is stable. The experimental results show that the SnO_2@CuO core-shell structure not only adsorbs NO more efficiently than single nanoclusters, but also has a 1.7 times higher degradation efficiency for methylene blue (MB).

Keywords: adsorption, nanostructure, nanoscale, core/shell.

1. INTRODUCTION

Environmental pollution has become more and more serious in recent years. To solve this problem, people have focused on nanocatalysts. Using photocatalytic properties of nanomaterials is an effective way to deal with pollution, especially water pollution [1 – 4]. Compared with traditional pollution treatment methods such as filtration, adsorption, and centrifugation, photocatalysis has several advantages because photocatalysts have higher catalytic efficiency, small reaction intervals, and will not produce secondary hazardous products [5, 6]. SnO_2 has a wide band gap [7], and SnO_2 is suitable as a photocatalyst due to the band gap of 3.6 eV, which corresponds to the activation of photons at a wavelength of 350 nm (UV-a range). Yu et al. [8] used SnO_2 to degrade methyl orange from water flowers under UV irradiation, and the methyl orange content decreased rapidly from 0 to 6 h, reaching 0 at 12 h. G. Ramanathan et al. [9] tested the degradation behavior of different dyes such as methylene blue, methyl orange, rhodamine B and textile dyes under light conditions, respectively, and the results showed that the catalytic degradation of methylene blue. The results showed a higher efficiency in catalytic degradation of MB. And CuO has also attracted the attention of researchers due to its excellent acoustic and photocatalytic activity and low cost for the degradation of dyes [10, 11].

Compared to single nanocatalysts, core-shell structured nanomaterial is a combination of multiple materials with controllable size structure, tunable multifunctional properties and high stability, which have received wide attention [12 – 14]. There are various methods to prepare core-shell structured materials, and nowadays, the synthesis methods include sol-gel method [15], hydrothermal method [16], precipitation method [17], etc. Astrini [18] et al. synthesized Au@AgAuS core-shell structured nanorods in successive synthesis steps and used them as photocatalysts for the photocatalytic oxidation of methylene blue under sunlight irradiation, and the experimental results demonstrated that the synergistic effect between the components exhibited excellent photocatalytic performance. Reddy [19] successfully synthesized CdS, ZnS and CdS/ZnS core-shell nanoparticles by a two-step synthesis method, and the results showed that the core-shell structured nanoparticles exhibited better photocatalytic activity than pure CdS and ZnS nanoparticles, and also the core-shell structured nanoparticles were recovered several times in the experiment and showed good stability.

Nowadays, there are few reports on SnO_2@CuO core-shell structures. In this paper, the crystal structure, electronic properties and small-molecule adsorption capacity of SnO_2@CuO nanocore-shell structures were investigated using first-principles calculations of density generalized theory, and experimental evidence was also performed. The results of the study can provide theoretical guidance for the related nano-core-shell structures.

2. CALCULATION DETAILS

2.1. Computational model

The space group of SnO_2 is $P4_2/mnm$. The lattice parameters of SnO_2 are $a = b = 4.7373$ Å, $c = 3.1864$ Å, $\alpha = \beta = \gamma = 90°$[20]. The lattice parameters of CuO are

* Corresponding author: X. Zhou
E-mail: *kmzxlong@kust.edu.cn*

a = 4.653 Å, b = 3.41 Å, c = 5.108 Å, α = γ = 90°, β = 99.5°[21]. All of them are in agreement with the experimental values. The core-shell structure was built using the Nanocluster cutout tool in Materials Studio 8.0. Based on the SnO_2 and CuO models, a sphere-like SnO_2 cluster model with a radius of 3 Å was cut out by nanocluster to replace the SnO_2 core, and a sphere like CuO cluster model with a radius of 6 Å was cut out to replace the CuO shell layer (see Fig. 1).

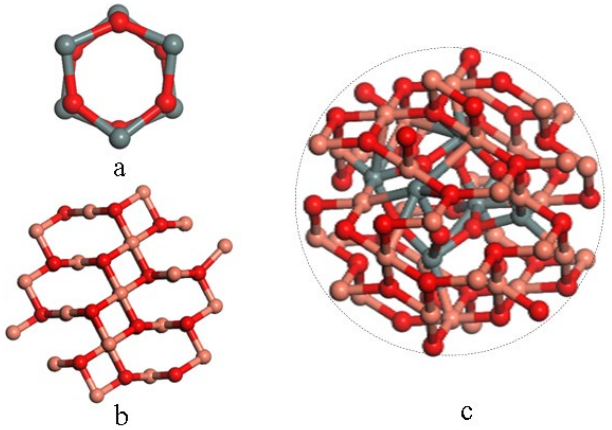

Fig. 1. a – SnO_2 nanoclusters; b – CuO nanoclusters; c – SnO_2@CuO core-shell structure

2.2. Calculation method

The SnO_2 cluster has 12 atoms, including 6 O-atoms and 6 Sn-atoms, the CuO cluster has 92 atoms, including 46 Cu-atoms and 46 O-atoms, and the SnO2@CuO core-shell structure has 89 atoms, including 39 Cu-atoms, 6 Sn-atoms and 44 O-atoms. The Dmol3 code of Materials Studio 8.0 based on density generalization theory [22] is used, and the specific calculation parameters are set as follows: the number of self-consistent iterations is 1000, convergence accuracy is fine, DND with d-orbit polarization is chosen [23], the errors caused by van der Waals forces are corrected by OBS, and the convergence accuracy of force and displacement are 0.04 Hartree/Å and 0.005 Å respectively, leaving the other values as default. The enthalpy and binding energy were generated and calculated for the model as follows:

$$\Delta_r H_m = \frac{E_{tot} - xE_{atom}(Cu) - yE_{atom}(Sn) - zE_{atom}(O)}{x+y+z}; \quad (1)$$

$$E_{coh} = \frac{E_{tot} - xE_{solid}(Cu) - yE_{solid}(Sn) - zE_{solid}(O)}{x+y+z}. \quad (2)$$

Since the first principles calculation is performed in the ground state (T = 0 K), the formulas for enthalpy of formation and binding energy can be obtained. Eq. 1 is for the enthalpy of formation and Eq. 2 is for the binding energy. E_{tot} is the total energy of SnO_2@CuO in the equilibrium state; E_{solid} and E_{atom} represent the energies of atoms in the ground state and free state, respectively; E (Cu), E (Sn) and E (O) are the energies of Cu, Sn and O atoms, respectively; x, y and z are the numbers of Cu, Sn and O atoms in the core-shell structure, respectively.

2.3. Experimental methods and materials

CuO nanopowders and SnO2@CuO core-shell nanomaterials were prepared by precipitation-calcination method, and using XRD and TEM characterize the microstructure and surface morphology of SnO_2@CuO core-shell nanomaterials. The photocatalytic and electronic properties of SnO_2@CuO core-shell nanomaterials were investigated by photocatalytic degradation of methylene blue, and the calculated results were verified.

3. RESULTS AND DISCUSSION

Table 1 lists the enthalpies of formation and binding energies of SnO_2 nanoclusters, CuO nanoclusters, and SnO_2@CuO core-shell structures, derived from structure optimization and energy calculations. The values in the table are negative, and it can be concluded that all three structures are able to exist stably based on the meaning of the enthalpy of formation and binding energy.

Table 1. Enthalpy of formation and binding energy of SnO_2, CuO and SnO_2@CuO core-shell structures

	$\Delta_r H_m$, eV	E_{coh}, eV
SnO_2	-0.0296	-0.4067
CuO	-0.0162	-0.1068
SnO_2@CuO	-0.0188	-0.1480

3.1. Electronic properties

The outer electron structures of the elemental species contained in the SnO_2 nanoclusters, CuO nanoclusters and SnO_2@CuO core-shell structures are O-$2s^2$ 2p4, Cu-$3d^9$ $4s^1$, Sn-$4d^{10}$ $5s^2$ $5p^2$.According to Table 2, the formation of the SnO_2@CuO core-shell structure increases the number of positive charges received by all Sn atoms, but the negative charges gathered by O atoms due to Cu atoms decrease SnO_2@CuO core-shell structure formation decreases the number of positive charges received by all Cu atoms, but the negative charges gathered by O atoms due to Sn atoms increase, proving that the SnO_2@CuO core-shell structure decreases the surface activity of CuO by decreasing the potential of the external CuO shell layer and decreasing its work function, while increasing the potential of the internal SnO_2 core and increasing its work function, the surface activity of SnO_2 is greatly increased. As a result, the shell layer can better encapsulate the core and the SnO_2@CuO core-shell structure is more stable, thus playing a synergistic role in the core-shell structure.

Table 2. Partial charge transfer of SnO_2, CuO and SnO_2@CuO nanoclusters

	Species	Charge, e
SnO_2	Sn (2)	0.869
	O (8)	-0.874
CuO	Cu (2)	0.747
	O (6)	-0.688
SnO_2@CuO	Cu (2)	0.647
	O (6)	-0.799
	Sn (79)	1.742
	O (85)	-0.853

In order to identify the regions where electron transitions may occur in the core-shell structure of SnO_2

nanoclusters, CuO nanoclusters and SnO_2@CuO, and to clarify the molecular orbital information of the three systems, analyze the HOMO (Energy of Highest Occupied Molecular Orbital) and LUMO (Energy of Lowest Unoccupied Molecular Orbital) energy levels of the three. We calculated their HOMO and LUMO energy levels using Dmol3, as shown in Fig. 2. The energy difference between HOMO and LUMO levels, also known as band gap, is calculated. Among them, the band gap of SnO_2@CuO core-shell structure is 0.220 eV, which is significantly smaller than that of SnO_2 nanoclusters (3.6 eV) and CuO nanoclusters (1.5 eV), which may result in that the chemical stability of SnO_2@CuO core-shell structure is not as high as that of a single nanocluster. However, due to the small band gap value, the electrons will gain less energy to jump over the band gap and realize the photocatalytic process. Therefore, we believe that this is favorable for the photocatalysis of SnO_2@CuO core-shell structure.

Fig. 2 a shows the HOMO-equivalent orbital surface of SnO2, the spherical lone electron pair aggregation appears on the Sn atom at position (1). This indicates that the s-orbital of this Sn atom is the most active site on its surface. The O-atom (red) at position (2) shows an aggregation of spindle-shaped lone pairs formed by lone pairs in the p-orbitals. Fig. 1 b shows the LUMO equivalent orbital surface of SnO_2. The area of the lone electron pair region covering around the three Sn atoms at position (1) is very large, and the figure is the lowest energy empty orbital formed by the hybridization of the s and p orbitals in the three Sn atoms, indicating that this is the easiest site to obtain electrons. Also, the spherical lone electron pair aggregation appearing on the O-atom (red) at position (2) is, we believe, formed by the lone electron pair within the s-orbital in the O-atom.

Fig. 2 c shows the HOMO equivalent orbital surface of CuO, where a dumbbell-shaped cluster of lone electron pairs appears on the Cu atom at position (1). The d-orbital of this Cu atom is the most active site on its surface. The O-atom (red) at position (2) shows a spindle-shaped cluster of lone electron pairs in the p-orbitals. Fig. 2 d shows the LUMO equivalent orbital surface of CuO. The area of the lone electron pair region at position (1) covers two Cu atoms, and the area above one of the Cu atoms is larger, which is the lowest energy empty orbital formed by the hybridization of the s and p orbitals of the two Cu atoms, where the highest activity is easily obtained.

Fig. 2 e shows the HOMO equivalent orbital surface of the SnO_2@CuO core-shell structure, where the spherical lone electron pair aggregation appears on the Sn atom at position (1). Therefore, the s-orbital of this Sn atom is the most active site on the surface of the CuO nanocluster (2). Spindle-shaped lone electron pair aggregation due to lone electron pairs within the p orbital appears on the O-atom at position (a). Fig. 2 f shows the LUMO equivalent orbital surface of the SnO_2@CuO core-shell structure with the spindle-shaped lone pair aggregation due to the lone electron pair in the p-orbital on the O-atom at position (1). The Cu atom at position (2) shows a dumbbell-shaped lone pair aggregation, and the d orbital of this Cu atom is the most active site. The spherical lone electron pair aggregation is observed on the Sn atom at position (3), and the s orbital of the Sn atom is the most active site.

As shown in Fig. 2, the core-shell structure compared to the single nanocluster Sn and Cu atoms mainly lost electrons, but the lone electron pair aggregation regions for Sn and Cu atoms are reduced compared to single cluster. In addition, SnO_2@CuO nanomaterials have increased specific surface area, carry more active sites, and facilitate electron transfer between SnO_2 and CuO nanocrystals. Thus, the potential electron transfer mechanism of SnO_2@CuO core-shell structure is revealed.

3.2. NO adsorption of molecules on the crystal structure structure

We mainly discuss the adsorption of two NO molecules on the catalyst surface as follows: (1) the catalyst surface is attached to the N atom end of the NO small molecule; (2) the catalyst surface is connected to the O atom end of the NO small molecule[24]. Before adsorption, the bond length of NO small molecule after structure optimization is 1.63 Å. Usually, we can determine the stable adsorption position of NO molecule on the surface of the three by calculating the adsorption energy.

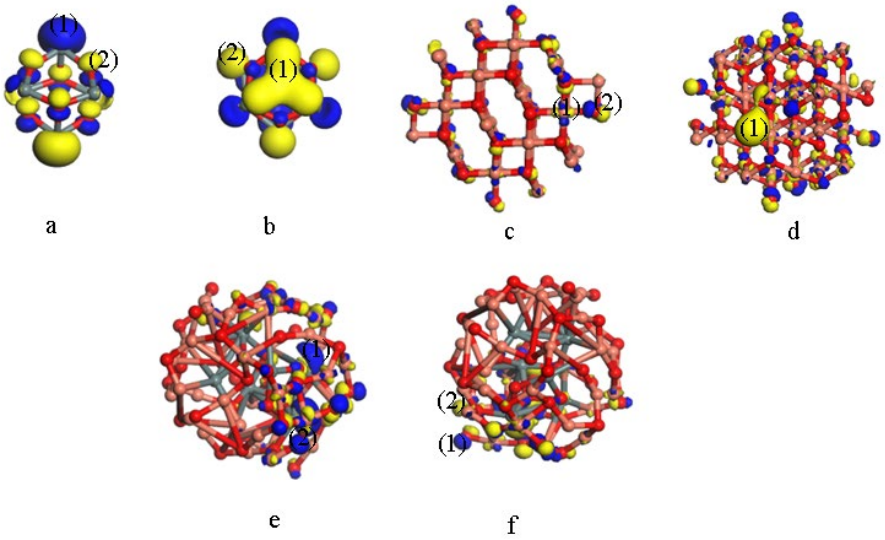

Fig. 2. SnO_2 nanoclusters: a – HOMO; b – LUMO orbital isosurface; CuO nanoclusters: c – HOMO; d – LUMO orbital isosurface; SnO_2@CuO core-shell structure: e – HOMO; f – LUMO orbital isosurface

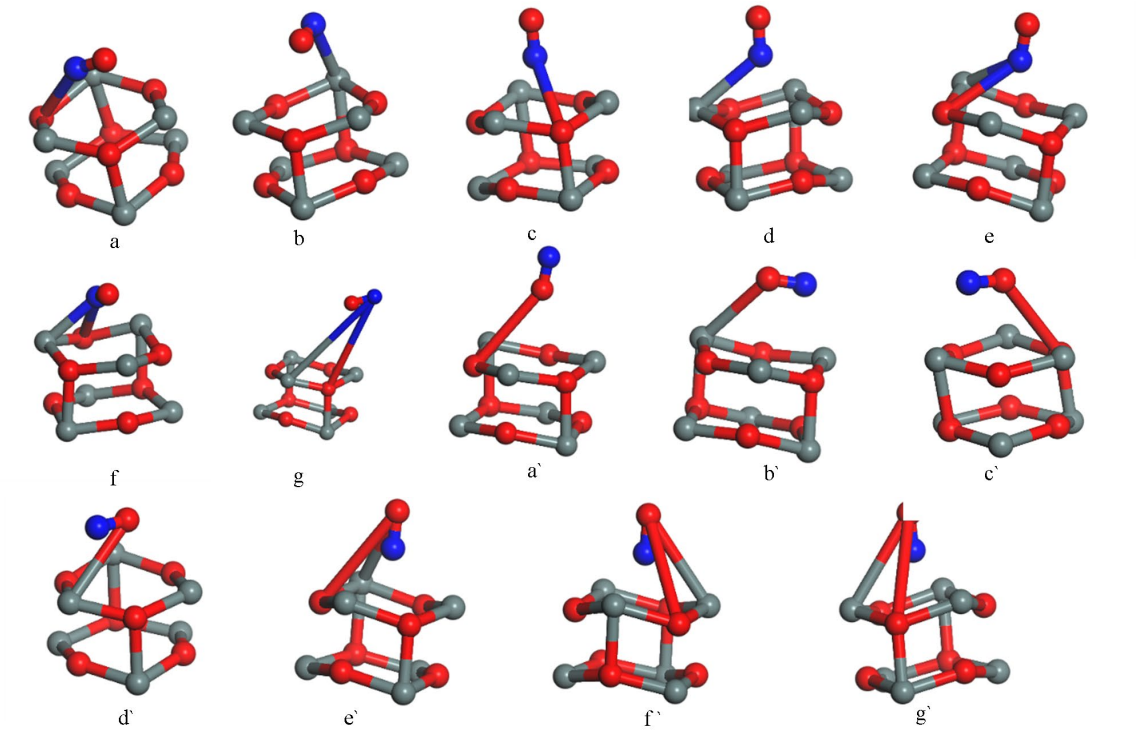

Fig. 3. a, b, c, d, e, f, g – side view of adsorption model of NO molecule on SnO_2 surface. The N atom of NO molecule is connected to the surface; a′, b′, c′, d′, e′, f′, g′ – the O atom of NO molecule is connected to the surface

The adsorption energy is calculated [25, 26] as follows:

$$E_{ads} = -(E_{Tot} - E_{mol} - E_{cat}), \quad (3)$$

where E_{Tot} is the total energy of the two after catalyst adsorption of NO molecules; E_{mol} is the energy of the NO molecules before NO adsorption; and E_{cat} is the energy of the catalyst surface.

3.2.1. Adsorption of NO molecules on SnO_2 nanocluster structures

Selecting seven positions as possible positions on the surface of the SnO_2 nanoclusters: the top position of O1 (1), the top position of Sn1 (2), the top position of O2 (3), the top position of Sn2 (4), the bridge position of O1-Sn1 (5), the bridge position of Sn1-O2 (6), the bridge position of O2-Sn2 (7). Thus, there are 14 adsorption configurations of NO molecules on the surface of SnO_2 nanoclusters (see Fig. 3). The parameters of the SnO_2@CuO core-shell structure were kept consistent in these models during the structure optimization process.

As shown in Fig. 4, the atom at the adsorption site, the bond length (dNO) of the NO small molecule and the adsorption energy are calculated [27]. Except for four positions (top-N atom of O1, Sn2 -O atom and bridge position of Sn1 -O2), the NO molecules form chemical bonds with the adsorption positions on the surface of SnO_2 nanoclusters with adsorption energies greater than 0.435 eV (42 KJ-mol^{-1}), and therefore all are chemisorbed [28]. The maximum adsorption energy (1.480 eV) was observed when NO molecules were adsorbed at the bridge site of Sn1-O2 on the surface of SnO_2 nanoclusters through the O-atom end.

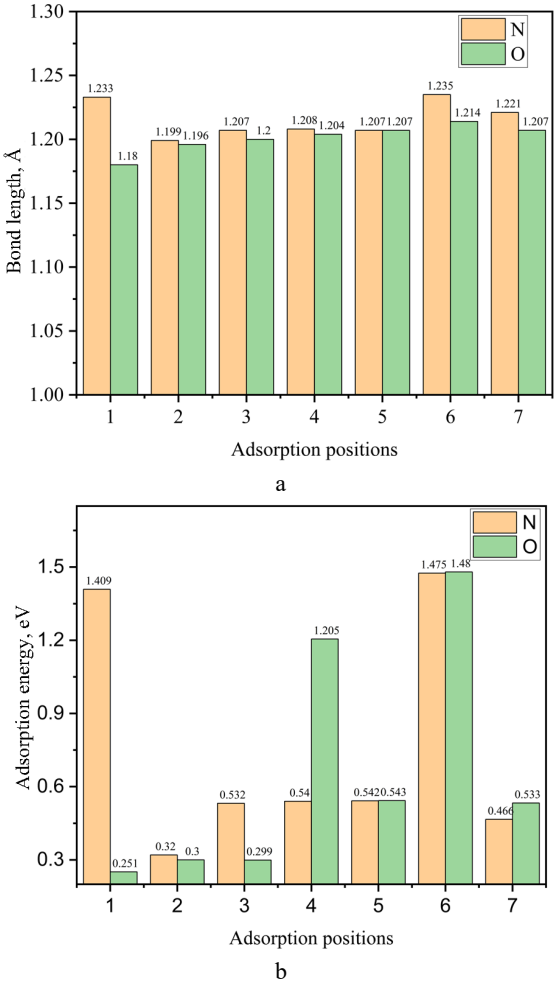

Fig. 4. a – the bond length of the NO small molecule (dNO); b – the adsorption energy (E_{ads}) on the surface of SnO_2 nanoclusters

The bond length change of NO molecules was observed, and it was found that the bond length of NO molecules decreased by about 0.4 Å when they were adsorbed on the surface of SnO_2 nanoclusters, indicating that the bonding of NO molecules became stronger during the adsorption process.

3.2.2. Adsorption of NO molecules on CuO nanocluster structures

Selecting eight positions as possible positions on the surface of the CuO nanoclusters: the top position of O1 (1), the top position of Cu1 (2), the top position of O2 (3), the top position of Cu2 (4), the bridge position of O1 – O1 (5), the bridge position of Cu1 – Cu1 (6), the bridge position of O2 – O2 (7), and the bridge position of Cu2 – Cu2 (8) [29 – 31]. Thus, there are 16 adsorption configurations of NO on the surface of SnO_2 nanoclusters[32] (see Fig. 5).

In order to fully understand the adsorption behavior of NO molecules on the surface of CuO nanoclusters, the bond length of the NO small molecule (dNO) and the adsorption energy (E_{ads}) are calculated as shown in Fig. 6.

The adsorption energy of NO molecules on the CuO nanocluster surface is less than 0.435 eV (42 KJ-mol^{-1}) except for two positions (Cu2 – Cu2 bridge site - N atom and O1 – O1 bridge site -O atom), which are physical adsorption. The maximum adsorption energy of 4.363 eV was observed when the NO molecules were adsorbed on the CuO nanocluster surface at the O1 – O1 bridge site at one end. The adsorption of NO molecules on CuO nanoclusters tends to be connected with N atoms.

3.2.3. Adsorption of NO molecules on the SnO_2@CuO nanoshell structure

Selecting eight positions on the surface of the CuO nanoclusters as possible positions: the top position of O1 (1), the top position of Cu1 (2), the top position of O2 (3), the top position of Cu2 (4), the bridge position of O1 – O1 (5), the top position of Cu1 – Cu1 (6), the top position of O2 – O2 (7), and the top position of Cu2 – Cu2 (8). There are 16 adsorption configurations of NO molecules on the surface of SnO_2@CuO nanoclusters (see Fig. 7).

In order to fully understand the adsorption behavior of NO molecules on the surface of SnO_2@CuO core-shell structure, the bond length of the NO small molecule (dNO) and the adsorption energy (E_{ads}) were calculated as shown in Fig. 8. From Fig. 8, the adsorption energy of NO molecule at each adsorption position on the SnO_2@CuO core-shell surface is greater than 1.4 eV. This indicates that strong chemisorption occurs on the surface of SnO_2@CuO core-shell structure.

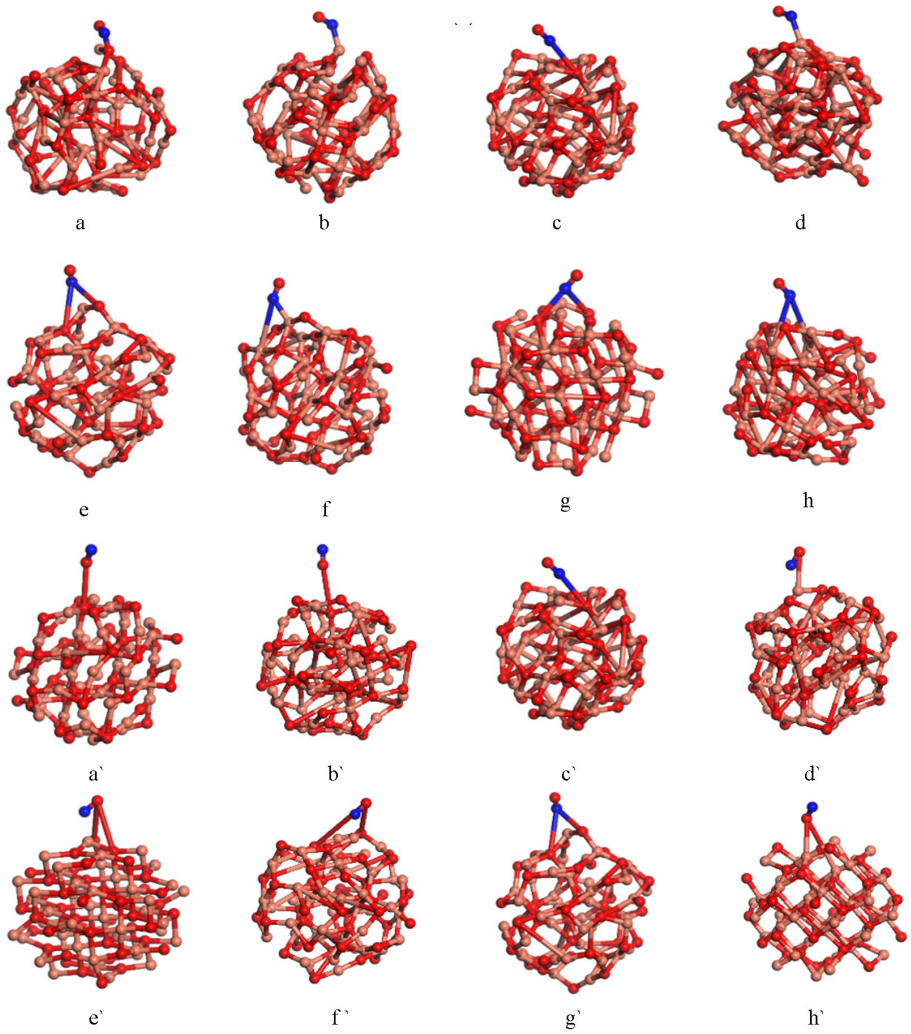

Fig. 5. a, b, c, d, e, f, g, h – side view of adsorption model of NO molecule on CuO surface. The N atom of NO molecule is connected to the surface; a′, b′, c′, d′, e′, f′, g′, h′ – the O atom of NO molecule is connected to the surface

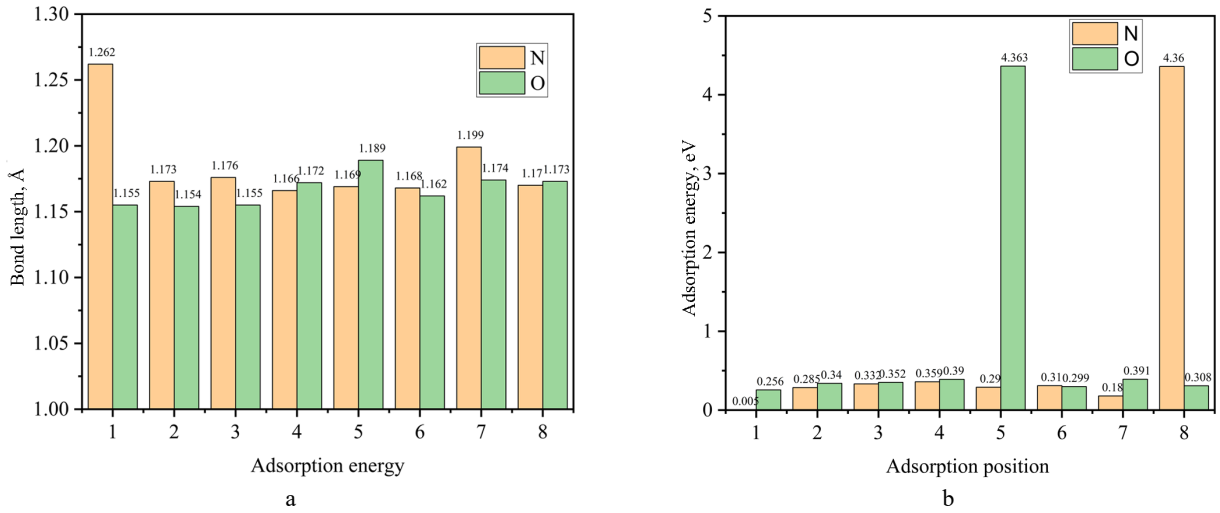

Fig. 6. a – the bond length of the NO small molecule (dNO); b – the adsorption energy (E_{ads}) on the surface of CuO nanoclusters

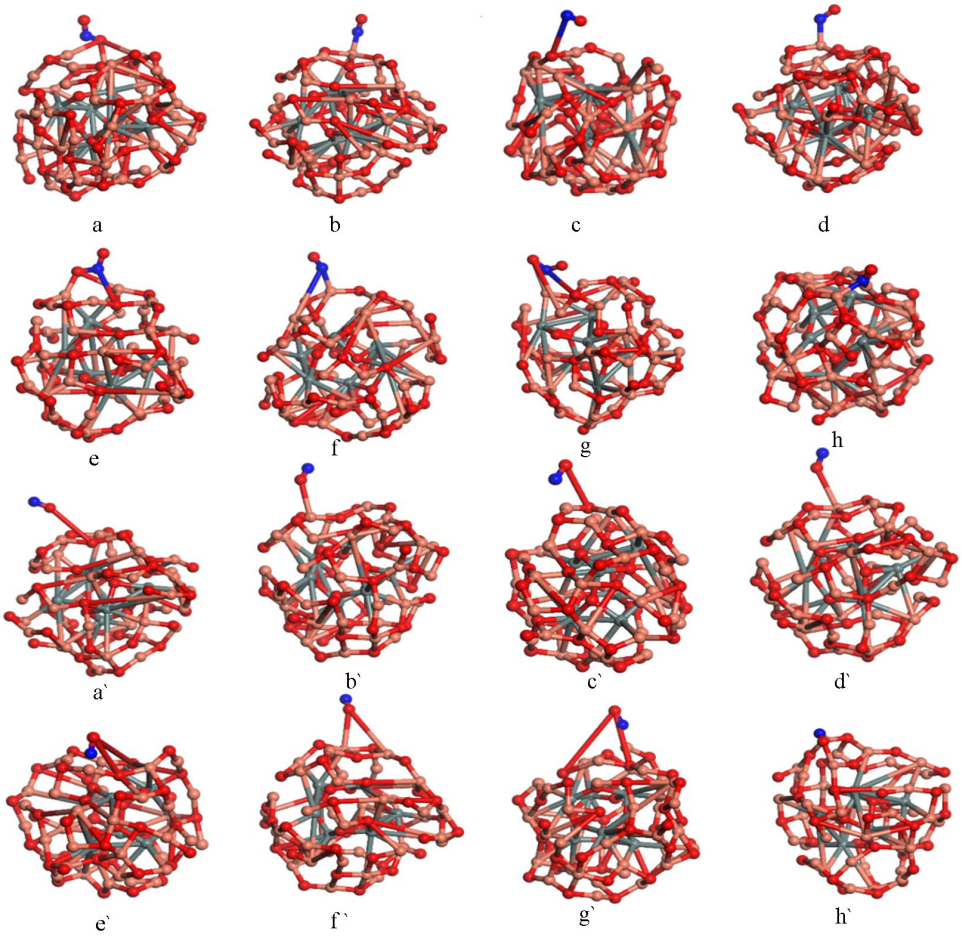

Fig. 7. a, b, c, d, e, f, g, h – side view of adsorption model of NO molecule on SnO_2@CuO surface. The N atom of NO molecule is connected to the surface; a′, b′, c′, d′, e′, f′, g′, h′ – the O atom of NO molecule is connected to the surface

The structure of NO small molecule is most stable when it adsorbs to the Cu1 – Cu1 bridge site on the surface of SnO_2@CuO core-shell structure through the N atom end. It was found that the bond lengths of NO molecules decreased by 0.4 – 0.5 Å when they were adsorbed on the surface of SnO_2@CuO core-shell structure, indicating that the bonding of NO molecules became stronger during the adsorption process. As for the adsorption of NO molecules on the SnO_2 nanoclusters, there is no significant difference between the adsorption of NO molecules attached with N or O atoms. Compared the adsorption energy of NO molecules on the surface of SnO_2 and CuO nanoclusters, it can be seen that the formation of the core-shell structure is effective in improving the adsorption capacity of adsorbed NO molecules overall, and the adsorption energy is very homogeneous, and the average value of the adsorption energy is equal to the maximum adsorption energy of a single nanocluster.

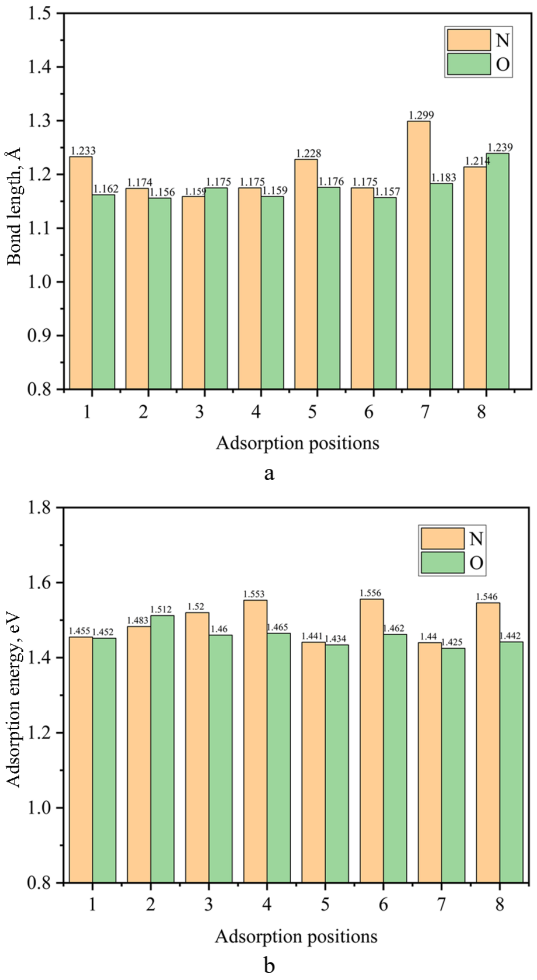

Fig. 8. a – the bond length of the NO small molecule (dNO); b – the adsorption energy (E_{ads}) on the surface of SnO_2@CuO nanoclusters

The average value of the adsorption energy is equal to the maximum adsorption energy of a single nanocluster. The bond length of NO molecules is reduced and the bond energy is enhanced compared to that of a single cluster.

4.1. XRD physical phase analysis of SnO_2@CuO core-shell nanostructures

The black powdered CuO, SnO_2@CuO samples were subjected to the physical phase analysis by XRD. As shown in Fig. 9, the CuO diffraction peaks of monoclinic crystalline system were observed at 2θ of 32.5°, 35.6°, 38.7°, 48.7°, 53.6°, 58.3°, 61.5°, 65.8°, 66.2°, and 67.9°, respectively. In addition to the CuO diffraction peak, the diffraction peaks of SnO_2 are shown at 2θ 26.6°, 33.9°, 38.9°, 51.8°, 54.8°, 57.8°, and 64.7° in Fig. 8. Therefore, we determine that the core-shell nanocomposites are composed of CuO and SnO_2.

4.2. TEM morphology analysis of SnO_2@CuO core-shell nanostructures

As shown in Fig. 10 a and b, TEM analysis of the SnO_2@CuO sample reveals that CuO shell layer is observed to be encapsulated on the SnO_2 core and the encapsulation layer is uniform.

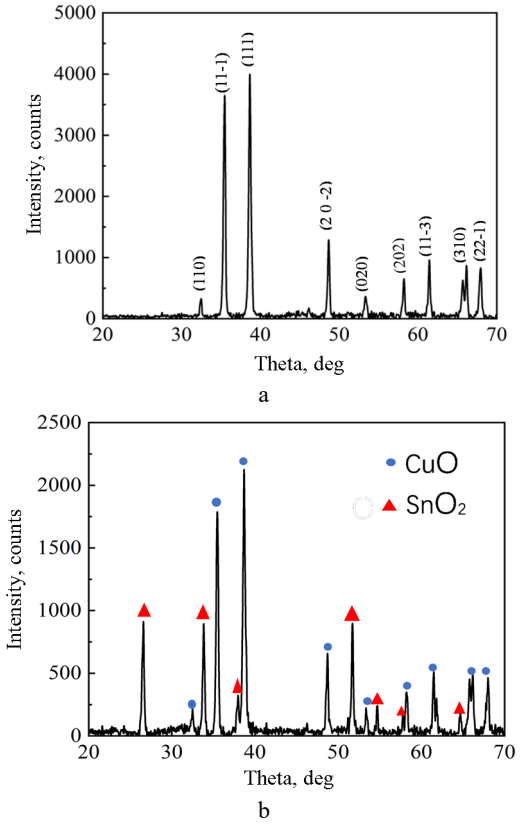

Fig. 9. a – XRD pattern of CuO nanopowders; b – XRD pattern of SnO_2@CuO core-shell structure

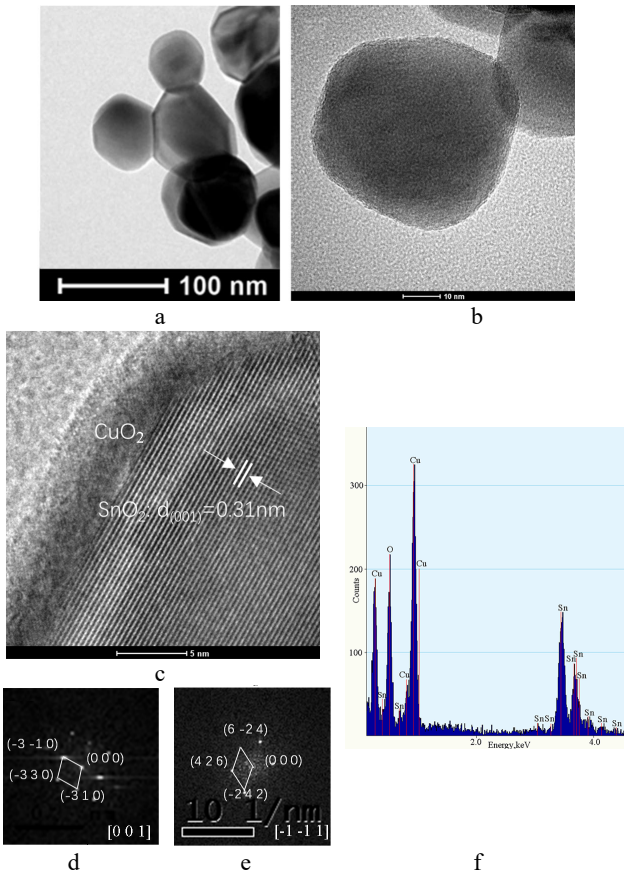

Fig. 10. TEM: a – CuO; b – SnO_2@CuO; c – high-resolution transmission electron micrograph of SnO_2@CuO; d – electron diffraction pattern of SnO_2; e – electron diffraction pattern of CuO; f – EDS energy spectrum

Due to the different lining of the samples, Fig. 10 c visualizes the core-shell structure of the samples covering the powder particles. In this figure, the centrally arranged lattice stripes are the core of the SnO_2 core-shell structure, and the dark gray lining material near the core is the shell layer CuO. Meanwhile, the presence of the interface is obvious, and the core SnO_2 and the shell layer CuO have different microscopic morphologies, but both of them have aligned crystal faces and diffraction spots.

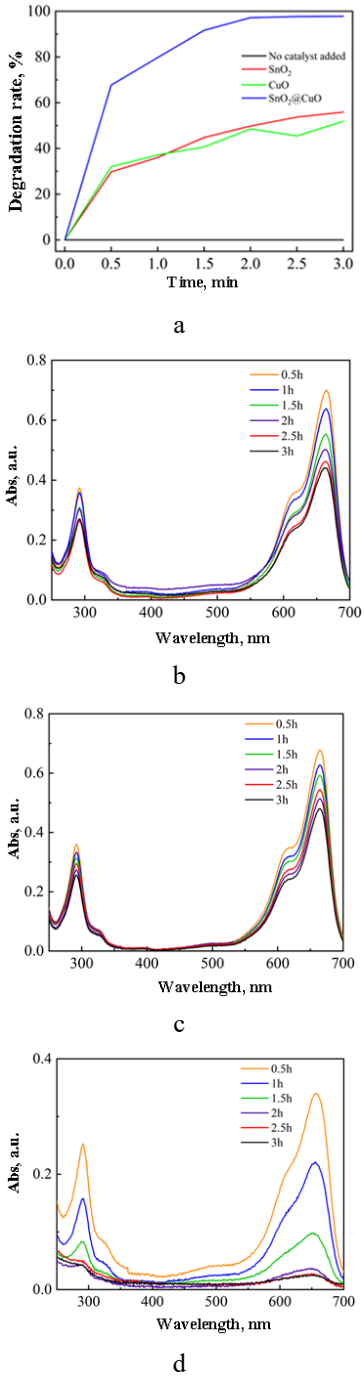

Fig. 11. a – reaction rate diagram of catalyst degradation of methylene blue; adsorption spectrum of: b – SnO_2; c – CuO; d – SnO_2@CuO nano core-shell to methylene blue solution

Fig. 10 d and e show the Fourier transform diffraction patterns of the HRTEM two-dimensional lattice phases of SnO_2 and CuO, respectively. Fig. 6 f shows the EDS energy spectrum of the SnO_2@CuO sample, which clearly shows that the core-shell structure is composed of Sn, O and Cu elements. The TEM analysis shows two regions of different phases in the nanoparticles, located in the core and shell regions, which excludes the possibility of the presence of any single-phase particles. Therefore, the core-shell structure nanophotocatalytic materials were successfully prepared experimentally using the precipitation-calcination method.

Fig. 11 b, c and d show the adsorption spectra of MB for three different catalysts, SnO_2, CuO and SnO_2@CuO, with the adsorption peak of MB located at around 665 nm.

The lower the peak of the absorbance of MB in the adsorption spectra, the lower the concentration of MB. As shown in Fig. 11 b, c and d, the intensity of the adsorption peaks at 665 nm for all three catalysts showed a decreasing trend with increasing degradation time. After 30 min of dark treatment, the intensities of the adsorption peaks at 665 nm for the MB solution changed to 0.998, 0.988 and 1.064, due to the adsorption of the catalysts on the MB solution, respectively.

The degradation efficiency of SnO_2@CuO composite material was 79.76 % after 1 h of xenon lamp irradiation, which was about twice as high as that of SnO_2 (36.07 %) and CuO (37.17 %) powders; the degradation efficiency of SnO_2@CuO composite material was 91.68 % after 2 h of xenon lamp irradiation, which was still higher than that of SnO_2 (44.79 %) and CuO (49.68 %) powders. After 3 h of xenon lamp irradiation, the degradation efficiency of SnO_2 was 55.91 %, the photocatalytic degradation efficiency of CuO was 51.90 %, and the degradation efficiency of SnO_2@CuO composite was 97.80 %. It indicates that all three have good catalytic activity for MB solution, but the catalytic efficiency of SnO_2@CuO core-shell material is significantly higher than that of SnO_2 and CuO materials, indicating that SnO_2@CuO core-shell material has better photocatalytic performance due to the interaction of SnO_2 and CuO.

4.4. Effect of different SnO_2@CuO content on photocatalytic degradation

The solutions containing 20 mg, 30 mg, 40 mg, and 50 mg of catalyst are shown in Fig. 12 a, which shows the adsorption spectra after 3 h of experimental testing. It can be seen that the degradation efficiency of the samples increased due to the increase of the catalyst content. After 3 h, the degradation rates of 20 mg, 30 mg, 40 mg and 50 mg catalysts were 98.66 %, 98.17 %, 99.46 % and 99.51 %, respectively. From the above data, it can be seen that in the reaction system of SnO_2@CuO core-shell material for MB degradation, the catalyst content changes significantly on the photocatalytic reaction rate of the samples. The increase of catalyst content can help to improve the rate of MB degradation solution. Fig. 12 b. The adsorption peak intensity of MB solution at 665 nm was 0.081, 0.06, 0.024 and 0.022, respectively, which showed that the change of adsorption peak intensity from 40 mg of catalyst tended to be flat.

From the above data, it can be seen that in the reaction system of SnO_2@CuO core-shell material for MB

degradation, the catalyst content caused a large variation in the degradation rate of the samples.

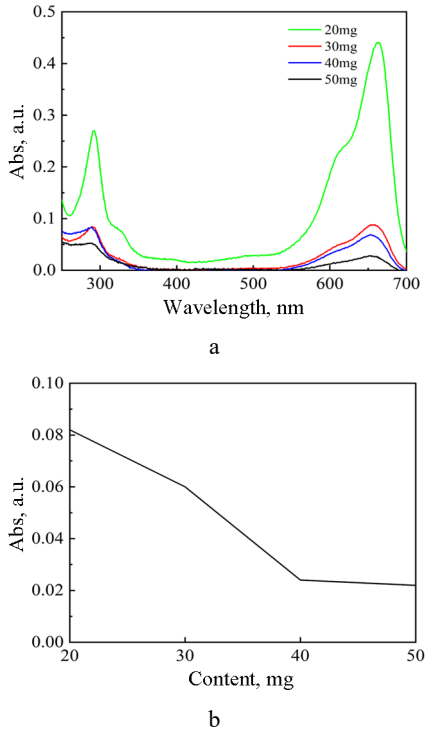

Fig. 12. Adsorption spectrum of SnO_2@CuO nano core-shell catalyst to methylene blue solution: a – absorption peak intensity variation spectra of MB solution under different wavelengths of visible light irradiation with different contents of SnO_2@CuO nano core-shell catalyst b – absorption peak intensity variation spectra of MB solution under 665nm visible light irradiation with different contents of SnO_2@CuO nano core-shell catalyst

When the light source conditions were kept constant, the increase of photocatalyst directly brought about a large number of electron-hole pairs, and a large number of hydroxyl radicals (OH) and superoxide ion radicals (O2-) appeared due to the formation of heterojunctions. While the MB to be degraded remains certain, the degradation rate must be increased. However, while the catalyst content increases, a large number of MB molecules are attached to the surface of SnO_2@CuO core-shell material resulting in the reduction of active sites on the photocatalyst surface, which reduces the utilization of visible light and OH radicals, leading to the reduction of catalytic efficiency. Therefore, in order to balance the relationship between the two and improve the catalytic efficiency, 50 mg of SnO_2@CuO core-shell material was selected for the experiments in this paper.

4.5 Photocatalytic mechanism

On the one hand, compared with SnO_2 and CuO single nano powders, SnO_2@CuO core-shell material increases the specific surface area of SnO_2@CuO core-shell material. The active site on its surface increases with the increase of the specific surface area, which ultimately improves the catalytic efficiency. On the other hand, the calculated bandgap of SnO_2@CuO core-shell material is 0.22 eV, which is much smaller than that of SnO_2 and CuO single nano powders, making the photocatalytic process easier to occur. In addition, heterojunction is formed in the core-shell structure, and the difference of Fermi level between the two substances improves the effective separation efficiency of the electron-hole pair, and further improves the catalytic efficiency of the core-shell structure. When the N-type semiconductor SnO_2 with a bandgap of 3.6 eV is in contact with the P-type semiconductor CuO with a bandgap of 1.5 eV, an built-in field from CuO to SnO_2 is formed due to the difference in fermi energy levels. When incident light irradiates SnO_2@CuO heterojunction, SnO_2 conduction band electrons migrate to CuO and holes migrate to SnO_2 under the action of electric field, realizing carrier separation and reducing the recombination rate, thus enhancing the photocatalytic activity and enhancing the photocatalytic degradation ability of SnO_2@CuO core-shell materials for MB.

5. CONCLUSIONS

The electronic properties of the three structures, SnO_2 nanoclusters, CuO nanoclusters and SnO_2@CuO core-shell structure, were investigated and compared by density functional theory calculations. After the formation of the core-shell structure, it is evident from the density of states diagram that the electronic states of both are not as active as those of the individual clusters due to the interaction between the core and the shell layer, thus maintaining the stability of the core-shell structure. Compared the adsorption of NO molecules by single SnO_2 and CuO nanoclusters, it was found that the adsorption capacity of the SnO_2@CuO core-shell structure was stronger for NO molecules, and the adsorption energy at each adsorption position was almost the same,the adsorption property is more stable.

SnO_2@CuO core-shell photocatalysts were prepared by precipitation-calcination method. The TEM and XRD analyses showed that the well-formed core-shell nanostructure were composed of two metal oxides, CuO and SnO_2. The photocatalytic degradation of the organic dye methylene blue using SnO_2 nanoclusters, CuO nanoclusters and SnO_2@CuO core-shell structure was obtained, and the degradation efficiency of SnO_2@CuO core-shell structure for methylene blue was 99.51 % reaching about 1.7 times higher than that of SnO_2 and CuO nanopowders. The core-shell nanostructures have great potential for catalysts.

Acknowledgments

We sincerely thank for Yunnan Fundamental Research Projects (grant number.202301AS070031). This work was supported by the Yunnan Fundamental Research Projects (grant number.202301AS070031).

REFERENCES

1. **Abd Elkodous, M.S., El-Sayyad, G., Abdel Maksoud, M.I.A., Kumar, R., Maegawa, K., Kawamura, G., Tan, W.K., Matsuda, A.** Nanocomposite Matrix Conjugated with Carbon Nanomaterials for Photocatalytic Wastewater Treatment *Journal of Hazardous Materials* 410 2021: pp. 124 – 657. https://doi.org/10.1016/j.jhazmat.2020.124657

2. **Zhu, H., Yuan, X., Yao, Q., Xie, J.** Shining Photocatalysis by Gold-Based Nanomaterials *Nano Energy* 88 2021: pp. 106 – 306. https://doi.org/10.1016/j.nanoen.2021.106306
3. **Yanushevska, O.I., Vlasenko, N.V., Telbis, G.M., Leonenko, E.V., Didenko, O.Z., Prozorovich, V.G., Ivanets, A.I., Dontsova, T.A.** Acid–Base and Photocatalytic Properties of TiO_2-Based Nanomaterials *Applied Nanoscience* 12 (3) 2022: pp. 691 – 700. https://doi.org/10.1007/s13204-021-01709-7
4. **Petronella, F., Truppi, A., Ingrosso, C., Placido, T., Striccoli, M., Curri, M.L., Agostiano, A., Comparelli, R.** Nanocomposite Materials for Photocatalytic Degradation of Pollutants *Catalysis Today* 281 2017: pp. 85 – 100. https://doi.org/10.1016/j.cattod.2016.05.048
5. **Singh, P., Mohan, B., Madaan, V., Ranga, R., Kumari, P., Kumar, S., Bhankar, V., Kumar, P., Kumar, K.** Nanomaterials Photocatalytic Activities for Waste Water Treatment: A Review *Environmental Science and Pollution Research* 29 (46) 2022: pp. 69294 – 69326. https://doi.org/10.1007/s11356-022-22550-7
6. **Mekonnen, M.M., Hoekstra, A.Y.** Global Gray Water Footprint and Water Pollution Levels Related to Anthropogenic Nitrogen Loads to Fresh Water *Environmental Science & Technology* 49 (21) 2015: pp. 12860 – 12868. https://doi.org/10.1021/acs.est.5b03191
7. **Aslam, M., Qamar, M.T., Ali, S., Rehman, A.U., Soomro, M.T., Ahmed, I., Ismail, I.M.I., Hameed, A.** Evaluation of SnO_2 for Sunlight Photocatalytic Decontamination of Water *Journal of Environmental Management* 217 2018: pp. 805 – 814. https://doi.org/10.1016/j.jenvman.2018.04.042
8. **Zhiyong, Y., Ruiying, Q., Huanrong, L., Zhiyin, W., Xiaohong, M., Chaonan, D.** Preparation and Photocatalytic Activity of SnO_2 *Materials Letters* 170 2016: pp. 25 – 30. https://doi.org/10.1016/j.matlet.2015.12.100
9. **Ramanathan, G., Murali, K. R.** Photocatalytic Activity of SnO_2 Nanoparticles *Journal of Applied Electrochemistry* 52 (5) 2022: pp. 849 – 859. https://doi.org/10.1007/s10800-022-01676-z
10. **Sahu, K., Satpati, B., Mohapatra, S.** Facile Fabrication of CuO Nanosheets for Photocatalytic Applications *Applied Physics A* 127 (5) 2021: pp. 361. https://doi.org/10.1007/s00339-021-04505-w
11. **Chauhan, M., Kaur, N., Bansal, P., Kumar, R., Srinivasan, S., Chaudhary, G.R.** Proficient Photocatalytic and Sonocatalytic Degradation of Organic Pollutants Using CuO Nanoparticles *Journal of Nanomaterials* 2020 (1) 2020: pp. 6123178. https://doi.org/10.1155/2020/6123178
12. **Zou, H., Luo, Z., Yang, X., Xie, Q., Zhou, Y.** Toward Emerging Applications Using Core–Shell Nanostructured Materials: A Review *Journal of Materials Science* 57 (24) 2022: pp. 10912 – 10942.
13. **Shafiee, A., Rabiee, N., Ahmadi, S., Baneshi, M., Khatami, M., Iravani, S., Varma, R. S.** Core–Shell Nanophotocatalysts: Review of Materials and Applications *ACS Applied Nano Materials* 5 (1) 2022: pp. 55 – 86. https://doi.org/10.1021/acsanm.1c03714
14. **Shiju, E., Abhijith, T., Narayana Rao, D.** Nonlinear Optical Behavior of Au@Ag Core- Shell Nanostructures *Journal of Molecular Liquids* 333 2021: pp. 115 – 935. https://doi.org/10.1016/j.molliq.2021.115935
15. **Bitaraf, M., Ghazi, M. E., Izadifard, M.** Studying Structural and Optical Properties of TiO_2–SnO_2 Core–Shell Synthesized by Sol–Gel Route *Crystal Research and Technology* 55 (3) 2020: pp. 190 – 0145. https://doi.org/10.1002/crat.201900145
16. **Zhu, Q., Zhang, X., Wang, X., Wu, X., Zhang, Z., Shen, J.** Hydrothermal Self-Assembled Fe_3O_4/CA Core-Shell Composites for Broadband Microwave Absorption *Journal of Magnetism and Magnetic Materials* 541 2022: pp. 168 – 511. https://doi.org/10.1016/j.jmmm.2021.168511
17. **Mahmoudi, E., Behnajady, M. A.** Synthesis of Fe_3O_4@NiO Core-Shell Nanocomposite by the Precipitation Method and Investigation of Cr(VI) Adsorption Efficiency *Colloids and Surfaces A: Physicochemical and Engineering Aspects* 538 2018: pp. 287 – 296. https://doi.org/10.1016/j.colsurfa.2017.11.020
18. **Pradyasti, A., Kim, D.S., Kim, M.H.** Synthesis of Au@AgAuS Core–Shell Hybrid Nanorods and Their Photocatalytic Application *Colloid and Interface Science Communications* 49 2022: pp. 100 – 635. https://doi.org/10.1016/j.colcom.2022.100635
19. **Reddy, Ch. V., Shim, J., Cho, M.** Synthesis, Structural, Optical and Photocatalytic Properties of CdS/ZnS Core/Shell Nanoparticles *Journal of Physics and Chemistry of Solids* 103 2017: pp. 209 – 217. https://doi.org/10.1016/j.jpcs.2016.12.011
20. **Mounkachi, O., Salmani, E., Lakhal, M., Ez-Zahraouy, H., Hamedoun, M., Benaissa, M., Kara, A., Ennaoui, A., Benyoussef, A.** Band-Gap Engineering of SnO_2 *Solar Energy Materials and Solar Cells* 148 2016: pp. 34 – 38. https://doi.org/10.1016/j.solmat.2015.09.062
21. **Guha, S., Peebles, D., Wieting, T.J.** Zone-Center (q =0) Optical Phonons in CuO Studied by Raman and Infrared Spectroscopy *Physical Review B* 43 (16) 1991: pp. 13092 – 13101. https://doi.org/10.1103/PhysRevB.43.13092
22. **Zhang, X., Gui, Y., Xiao, H., Zhang, Y.** Analysis of Adsorption Properties of Typical Partial Discharge Gases on Ni-SWCNTs Using Density Functional Theory *Applied Surface Science* 379 2016: pp. 47 – 54. https://doi.org/10.1016/j.apsusc.2016.04.048
23. **Inada, Y., Orita, H.** Efficiency of Numerical Basis Sets for Predicting the Binding Energies of Hydrogen Bonded Complexes: Evidence of Small Basis Set Superposition Error Compared to Gaussian Basis Sets *Journal of Computational Chemistry* 29 (2) 2008: pp. 225 – 232. https://doi.org/10.1002/jcc.20782
24. **Ren, J., Song, K., Li, Z., Wang, Q., Li, J., Wang, Y., Li, D., Kim, C.K.** Activation of Formyl CH and Hydroxyl OH Bonds in HMF by the CuO(1 1 1) and Co3O4(1 1 0) Surfaces: A DFT Study *Applied Surface Science* 456 2018: pp. 174 – 183. https://doi.org/10.1016/j.apsusc.2018.06.120
25. **Yoon, S.H., Kang, U., Park, H., Abdel-Wahab, A., Han, D.S.** Computational Density Functional Theory Study on the Selective Conversion of CO_2 to Formate on Homogeneously and Heterogeneously Mixed $CuFeO_2$ and CuO Surfaces *Catalysis* 335 2019: pp. 345 – 353. https://doi.org/10.1016/j.cattod.2018.12.043
26. **Cao, Z., Zhang, W., Ding, R., Wang, J., Pu, M., Yang, Z., Lei, M.** The Reaction Paths of CH2O Decomposition on CuO(111) Surface: A DFT Study *Journal of Physical Organic Chemistry* 33 (1) 2020: pp. 40.

https://doi.org/10.1002/poc.4017

27. **Zhang, J., Zhang, R., Wang, B., Ling, L.** Insight into the Adsorption and Dissociation of Water over Different CuO(111) Surfaces: The Effect of Surface Structures *Applied Surface Science* 364 2016: pp. 758 – 768. https://doi.org/10.1016/j.apsusc.2015.12.211
28. **Yu, X., Zhao, C., Zhang, T., Liu, Z.** Molecular and Dissociative O_2 Adsorption on the $Cu_2O(111)$ Surface *Physical Chemistry Chemical Physics* 20 (31) 2018: pp. 20352 – 20362. https://doi.org/10.1039/C8CP03035A
29. **Yu, X., Zhang, X., Wang, H., Feng, G.** High Coverage Wat er Adsorption on the CuO(111) Surface *Applied Surface Sci ence* 425 2017: pp. 803 – 810. https://doi.org/10.1016/j.apsusc.2017.07.086
30. **Yu, X., Zhang, X.** High Coverage Water Adsorption on CuO(011) Surface *Physical Chemistry Chemical Physics* 19 (28) 2017: pp. 18652 – 18659. https://doi.org/10.1039/C7CP03003G
31. **Suo, W., Sun, S., Liu, N., Li, X., Wang, Y.** The Adsorption and Dissociation of N_2O on CuO(111) Surface: The Effect of Surface Structures *Surface Science* 696 2020: pp. 121 – 596. https://doi.org/10.1016/j.susc.2020.121596
32. **Hu, R., Zhou, X., Yu, J.** The Effect of Surface Structure on Ag Atom Adsorption over CuO(111) Surfaces: A First Principles Study *Applied Surface Science* 425 2017: pp. 1111 – 1117. https://doi.org/10.1016/j.apsusc.2017.07.141